Oil & Gas Science and Technology – Rev. IFP, Vol. 61 (2006), No. 4, pp. 515-525

IFP International Conference
Rencontres scientifiques de l'IFP

Research Advances in Rational Design of Catalysts and Sorbents
Avancées de la recherche dans la conception rationnelle de catalyseurs et d'adsorbants

Dual Effect of H_2S on Volcano Curves in Hydrotreating Sulfide Catalysis

N. Guernalec[1], C. Geantet[1], P. Raybaud[2], T. Cseri[3], M. Aouine[1] and M. Vrinat[1]

1 IRC-CNRS, 2 avenue Albert Einstein, 69626 Villeurbanne - France
2 Institut français du pétrole, Direction Chimie et Physico-chimie Appliquées, 1-4 avenue de Bois-Préau, 92858 Rueil-Malmaison - France
3 IFP-Lyon, Direction Catalyse et Séparation, BP 3, 69390 Vernaison - France
e-mail: nadege.guernalec@catalyse.cnrs.fr - christophe.geantet@catalyse.cnrs.fr - pascal.raybaud@ifp.fr tivadar.cseri@ifp.fr - aouine@catalyse.cnrs.fr - vrinat@catalyse.cnrs.fr

Résumé — Effet dual d'H_2S sur les courbes en volcan en catalyse d'hydrotraitement — Les progrès récents des techniques de modélisation moléculaire quantique ont permis l'interprétation rationnelle des tendances périodiques observées en catalyse par les sulfures de métaux de transition. Les courbes en volcan obtenues de façon empirique peuvent être expliquées par des modélisations microcinétiques intégrant des descripteurs chimiques judicieux calculés *ab initio*. Cette approche a été appliquée avec succès en catalyse d'hydrotraitement en utilisant l'énergie de liaison metal-soufre comme descripteur *ab initio*. L'objectif du présent travail était d'étendre cette approche en explorant les effets des conditions réactionnelles (pression partielle en H_2S) sur les courbes en volcan. Dans ce but, les images de microscopie électronique à transmission haute résolution (METHR) combinées à la modélisation moléculaire des morphologies et des surfaces présentes ont permis de fournir une évaluation du nombre de sites potentiellement actifs. Cette approche est illustrée dans le cas du sulfure de cobalt supporté et non supporté. Un modèle microcinétique amélioré permet d'interpréter l'effet dual de l'H_2S observé en hydrogénation du toluène: effet inhibiteur pour les sulfures MoS_2, Rh_2S_3, RuS_2, NiMoS et effet promoteur pour les sulfures Cr_2S_3 et Co_9S_8. Les résultats expérimentaux combinés à la modélisation cinétique montrent que la position du maximum de la courbe en volcan correspondant au catalyseur optimal le plus performant dépend des conditions du milieu réactionnel.

Abstract — Dual Effect of H_2S on Volcano Curves in Hydrotreating Sulfide Catalysis *— Recent progresses achieved by quantum molecular modeling techniques enabled the rational interpretation of catalytic trends of series of transition metal sulfide catalysts. Empirical volcano curves can be explained by microkinetic models including chemical descriptors calculated at an ab initio level. This approach was successfully applied in the field of hydrotreating catalysis using the metal-sulfur bond energy descriptor. The purpose of the present work was to extend this approach by exploring the effect of reaction conditions (partial pressure of H_2S) on the volcano curve. On the one hand, high resolution transmission electron microscopy (HRTEM) images combined with molecular modeling of morphologies and surfaces exposed by catalysts provide an estimate of the number of potential active sites. This approach is illustrated for the relevant case of unsupported or alumina supported Co_9S_8 sulfide. On the other hand, an improved microkinetic model is proposed in order to reflect the dual effects of H_2S observed in the hydrogenation of toluene : an inhibiting effect for MoS_2, Rh_2S_3, RuS_2, NiMoS and a promoting effect for Cr_2S_3 et Co_9S_8. The experimental results and kinetic modeling reveal that the maximum of the volcano curve and thus the optimal sulfide catalyst depends closely on the partial pressure of H_2S.*

INTRODUCTION

In the field of heterogeneous catalysis, volcano curves play a key role for correlating catalytic activities with intrinsic properties of catalysts such as its ability to form chemical bonds with reactants, products or intermediates [1-3]. With the tremendous progress of ab initio molecular modeling techniques within the framework of density functional theory (DFT), the origin of volcano curves can be explained by using ab initio calculated chemical descriptors directly linked to intrinsic properties of catalysts.

The experimental data and the chemical descriptors are connected with the help of Brønsted-Evans-Polanyi relationships [4, 5] and kinetic model using Langmuir-Hinshelwood (LH) formalism. This approach may offer a powerful guideline for the design of new catalysts.

Such volcano curves were obtained for hydrotreating catalysts [6], using the sulfur-metal bond energy descriptor, called *E(MS)*, as defined in [7, 8]. A good fitting between predicted and experimental hydrodesulfurization (HDS) of dibenzothiophene (DBT) was obtained for a series of sulfides catalysts [9], with the use of a kinetic equation based on a Langmuir-Hinshelwood equation assuming that the reactant (dibenzothiophene) and H_2S compete on the same catalytic site. Without any assumption on the adsorption mode of H_2S and H_2, this model provided a rational explanation of the origin of volcano curves in HDS catalysis.

More complex kinetic pathways including H_2 and H_2S dissociative activation on the catalytic sites have been proposed for the interpretation of the kinetic orders with respect to H_2S determined on conventional Co(Ni)MoS catalysts [10-12]. In fact, H_2S acts as an inhibitor on conventional systems based on Mo or W disulfides as also observed on unconventional sulfide active phases such as Pd, Ru, Rh [13, 14].

In contrast, recent results demonstrate that H_2S may also enhance the turnover rate in toluene hydrogenation in the case of Cr_2S_3 catalyst [15].

In the present paper, we first show that this positive effect of H_2S also occurs over unsupported and over alumina supported cobalt sulfide, pointing out the fact that sulfides with low *E(MS)*, exhibit a specific behavior with respect to H_2S. As announced in [15], we propose an improvement of the kinetic model able to explain this positive effect of H_2S. At the same time, we propose an approach combining high resolution transmission electron microscopy (HRTEM) and molecular modeling of morphologies and surfaces exposed for a selected TMS series (MoS_2, Rh_2S_3, RuS_2, NiMoS, Cr_2S_3 and Co_9S_8) to estimate the number of potential active sites of the sulfides catalysts.

This approach enabling a more rigorous normalization of turnover rate will be illustrated in detail for the case of Co_9S_8.

1 EXPERIMENTAL

1.1 Catalysts Preparation

1.1.1 Unsupported Cobalt Sulfide

Unsupported cobalt sulfide was prepared at room temperature by addition drop by drop of Na_2S in a $Co(NO_3)_2$,6 H_2O aqueous solution [16]. The powder obtained was filtered, washed with water and dried in a N_2 flow. Then, the solid was heated in a 15% H_2S/H_2 flow at 713 K during 4 h. The specific surface area of the sample is 40 m^2/g. Its composition according to chemical analysis (S/Co atomic ratio of 0.9) and XRD pattern corresponds to a Co_9S_8 phase.

1.1.2 Supported Samples

Co supported catalyst (14.8 wt% of Co) was prepared by pore-filling impregnation of a γ-Al_2O_3 support (surface area: 240 m^2/g and pore volume: 0.61 cm^3/g) with an aqueous solution of $Co(NO_3)$,6 H_2O. The catalyst was dried overnight at room temperature and during 10 hours at 373 K. Subsequently this material was calcined at 673 K for 4 h in a flow of air (100 cc/min), then sulfided at 673 K for 4 h in a 15% H_2S/H_2 flow.

The Mo, Ru, Rh and Cr supported catalysts were prepared by the same method using respectively $(NH_4)_6Mo_7O_{24}$,4H_2O, $RuCl_3$, $[(NH_3)_5Rh]Cl_3$ and $Cr(NO_3)_3$ precursor salts. Metal loadings of each sample are reported in Table 1. However, only Mo and Rh catalysts were calcined respectively at 673 K for 4 h and 523 K for 1 h in a flow of air. After all the catalysts were sulfided: Ru and Rh in a 15% H_2S/N_2 flow at 673 K for 4 h; Mo and Cr in a 15% H_2S/H_2 flow at 673 K for 4 h. It is important during the activation procedure to avoid a too reductive atmosphere in the case of Ru and Rh to obtain the fully sulfided state [17].

1.2 Catalysts Characterization and Modeling

1.2.1 Characterization

Several techniques such as TEM combined with EDS (Jeol 2010, point to point resolution 0.19 nm), C-S analysis (Juwe), XRD (Bruker D5005) and chemical analysis were used for the characterization of the catalysts. Particle sizes estimated from TEM and S/M ratio are reported in Table 1.

1.2.2 Molecular Modeling of Surfaces and Morphologies

Modeling of sulfide surfaces and morphologies was carried out using the "Crystal Builder" and "Surface Builder" modules of Cerius^2 interface [18]. The (hkl) surfaces corresponding to the planes observed by transition electron microscopy (TEM) have been built in two steps: the sulfides crystal is created from the conventional cell with the "Crystal Builder" module, then the crystal is cleaved in the (hkl) direction with

the "Surface Builder" module. Depending on the surface orientations, there may exist non equivalent choices for the cleavage plane. *Ab initio* calculations of surface energies help for determining the thermodynamic stability of surface: this has been undertaken in previous studies for MoS_2, Co(Ni)MoS [19, 20] and RuS_2 surfaces [21, 22]. However, such a systematic investigation for the whole sulfide series explored in the experimental section was beyond the scope of the present work. In a first approximation, the most probable exposed surface was chosen as the one minimizing the total number of cleaved bonds (sulfur-metal, metal-metal and sulfur-sulfur). In the future, it can be expected that new *ab initio* results will enable a more precise determination of surfaces stability.

TABLE 1

Characteristics of the supported TMS ordered as a function of the sulfur-metal bond descriptor, *E(MS)*, as defined in [9]

Catalyst	Metal loading (% wt.)	Estimated particle size (nm)	S/Me atomic ratio	E(MS) (kJ/mol)
MoS_2/Al_2O_3	10.2	2	2.3	166
RuS_2/Al_2O_3	5.4	2.5	2.3	141
$NiMo/Al_2O_3$	9.3 (Mo), 2.4 (Ni)	2	1.8	128
Rh_2S_3/Al_2O_3	0.9	2	1.3	119
Co_9S_8/Al_2O_3	6.3	10	1.1	111
Cr_2S_3/Al_2O_3	3.2	5	1.3	97

The ideal particle morphologies have been modeled using the Gibbs-Curie-Wulff law connecting surface energies and particle morphology *(Equations 1 and 2)*.

$$\frac{\Gamma_{hkl}}{d_{hkl}} = \frac{\Gamma_{h'k'l'}}{d_{h'k'l'}} \quad (1)$$

$$\Gamma_{hkl} S_{hkl} = \Gamma_{h'k'l'} S_{h'k'l'} \quad (2)$$

Γ_{hkl} surface energy of (hkl) plane exposed on the particle surface,

d_{hkl} distance between the (hkl) surface and the particle centre,

S_{hkl} area of the (hkl) plane exposed on the particle.

For MoS_2 and Co(Ni)MoS surfaces, surface energy values and morphologies are already solved by previous *ab initio* calculations [23, 24]. However, for other sulfides, *ab initio* data are not available. Without knowing the surface energy values of the surfaces exposed by the different transition metal sulfides, hypothetical morphologies have been created using the "Morphology" module of Cerius^2 (by varying arbitrarily Γ_{hkl}) to generate crystallites morphologies exposing the surfaces observed by HRTEM. For each morphology, we deduce the relative area of the different (hkl) surfaces which is the important insight for determining the surface density of sites.

1.2.3 Active Sites Counting

The analysis of the surface coordination of all atoms belonging to the surface is carried out in order to determine the number of sulfur-metal, sulfur-sulfur and metal-metal bonds. After cleavage, we considered as a potentially catalytically active site, the transition metal atoms verifying the following rules:

- the transition metal atom is a Coordinatively Unsaturated Sites (CUS) exhibiting at least one sulfur vacancy,
- the transition metal atom possesses one sulfur neighbor on the catalytic surface.

The surface concentration of potential active sites for the (hkl) surface is determined by the following relationship:

$$[AS]_{hkl} = \frac{N_{hkl}}{S_{hkl}} \quad (3)$$

N_{hkl} number of potentially active sites for a define (hkl) surface by simulation cell,

S_{hkl} area of the (hkl) surface in the simulation cell.

The average number of potential active sites per particle is deduced:

$$[AS]_p = \sum_{hkl} S_{hkl} [AS]_{hkl} = \sum_{hkl} x_{hkl} S_p [AS]_{hkl} \quad (4)$$

x_{hkl} proportion of the (hkl) surface for the given morphology,

S_p total surface area of the particle for the given morphology.

The estimate of particle sizes obtained by TEM *(Table 1)* is used to deduce the value of S_p according to 3D morphological models adapted for each sulfide. The morphologies and values of x_{hkl}, $[AS]_{hkl}$ and $[AS]_p$ are reported in Table 2 for all sulfides.

1.3 Catalytic Tests

Hydrogenation (HYD) of toluene is used as a model reaction to determine the catalytic activities of the catalysts. The test was performed under dynamic conditions with various H_2S partial pressures, obtained by dilution of H_2S/H_2 standard mixtures, in the following conditions: $P_{total} = 3.5 \times 10^3$ kPa, Total flow rate = 80 mL/min, $P_{Toluene} = 5.6$ kPa and $T_{reaction} = 623$ K. Specific activity was measured, according to first-order kinetics, after 15 h on stream when the steady state is reached. Activities are accurate to within 10%. Different relevant levels of H_2S partial pressures were chosen in the range of 0.52 to 12 kPa. The procedure was described in detail in [15].

2 RESULTS AND DISCUSSION

2.1 Effect of H_2S on the Catalytic Activity

In our previous study [15], we observed a positive kinetic order with respect to H_2S for Cr_2S_3 which is localized on the ascending branch of the volcano curve corresponding to low

TABLE 2

Analysis of the morphology and site density for the supported sulfide catalysts

Catalyst	Morphology	Surfaces (hkl): proportion	Density of sites $[AS]_{hkl}$ (per nm^2 of (hkl) surface)		Active sites (mol per g)
Co_9S_8/Al_2O_3		$(0\bar{2}2)$: 25%	2.9		
		(422) : 25%	3.3	3.5*	0.5×10^{20}
		$(1\bar{3}1)$: 25%	5.9		
		(111) : 25%	2.0		
RuS_2/Al_2O_3		(111) : 25%	6.3		
		(010) : 25%	6.3	5.7	1.1×10^{20}
		(102) : 25%	5.7		
		(110) : 25%	4.5		
Rh_2S_3/Al_2O_3		(211) : 59%	5.8		
		(123) : 38%	5.8	5.8	0.5×10^{20}
		$(1\bar{3}1)$: 3%	4.8		
Cr_2S_3/Al_2O_3		(002) : 93%	1.4		
		(110) : 3.5%	6.9	1.7	4.5×10^{20}
		$(1\bar{1}0)$: 3.5%	4.0		
MoS_2/Al_2O_3		$(10\bar{1}0)$: 48%	2.5		
$NiMo/Al_2O_3$		$(\bar{1}010)$: 48%	2.5	2.4	2.0×10^{20}
		(010) : 4%	0.0		

* $[AS]_p$: average number of site density (expressed per nm^2 of particle).

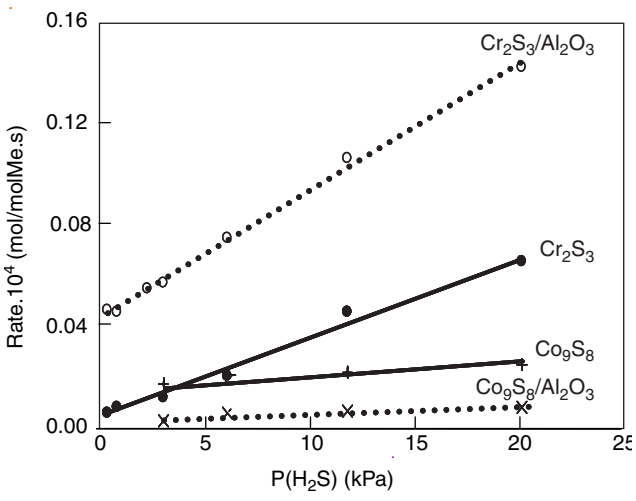

Figure 1

Effect of H_2S partial pressure on the catalytic conversion of toluene on Al_2O_3 supported and non supported Cr_2S_3 and Co_9S_8 catalysts.

E(MS) values. Co_9S_8 also belongs to this region of the volcano curve according to the sulfur-metal bond energy descriptor [7-9]. As shown in Figure 1, the supported Co sulfide catalyst slightly increases its catalytic activity when H_2S partial pressure increases even if it is to a lesser extent than for Cr_2S_3. The kinetic order with respect to sulfur is 0.13. Unsupported Co_9S_8 showed also the same trend (kinetic order 0.18) evidencing that it is an intrinsic property of this cobalt sulfide phase.

For Mo, Ru and Rh sulfides supported over alumina, the inhibiting effect of H_2S has been reported [10, 15] and was found to vary in the following order Mo < Ru < Rh. These previous data will be used for comparison with the cobalt catalyst.

2.2 Morphology of Sulfide Particles

In order to investigate the crystallographic surfaces involved in the catalytic reaction, HRTEM was performed on the different catalysts. In what follows, we focus on the case of cobalt sulfides. A similar approach was used for all other sulfides.

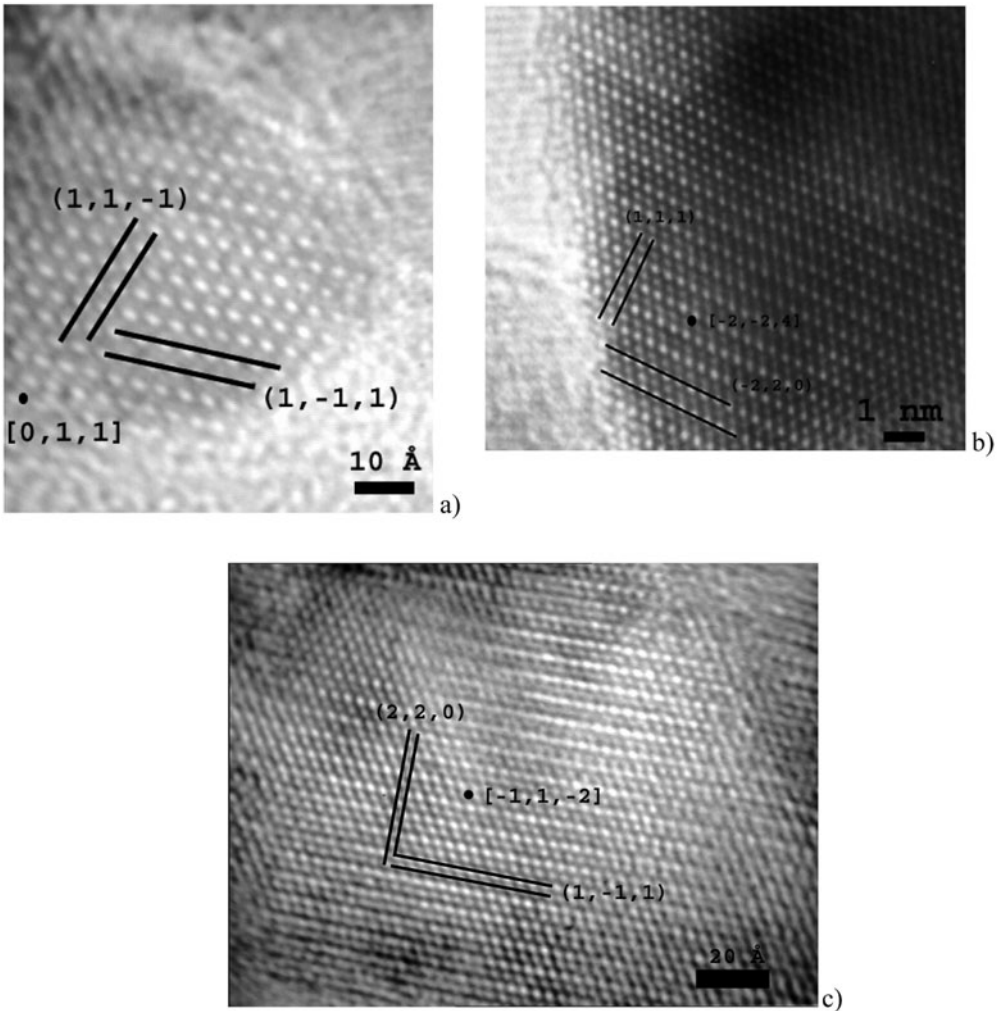

Figure 2

HRTEM images of Co_9S_8 bulk catalyst observed under various orientations a) [0,1,1] , b) [-2,-2,4] and c) [-1,1,2].

For unsupported Co_9S_8 several atomic resolution images were obtained as illustrated in Figure 2. Statistical analysis on the particle size, average description of zone axis and surface planes were combined with the modeling of the active surface and morphology description of the particles. Thus, the geometrical model of an active particle can be obtained and the surface concentration of potentially active sites numbered as illustrated in Figure 3.

This systematic approach was also performed on the supported cobalt catalyst, and example of HRTEM image obtained is illustrated in Figure 4. For this sample, only one zone axis [211] was observed suggesting that a preferential orientation exits through an orientation relationship (400) of Al_2O_3 and (422) of Co_9S_8 with a small lattice misfit between the two planes (0.202 nm and 0.1985 nm respectively). This epitaxial effect gives rise to a different morphology for the supported Co_9S_8 particles as illustrated in Figure 5.

This crystallographic analysis was extended to all the supported samples and allowed us to determine for each system the morphology representative for the different exposed surfaces and the concentration of active sites. Table 2 reports all information for the morphology and surface site counting. It can be noticed that all supported TMS exhibit the same range of active site concentration (when expressed per gram of catalyst). In contrast, catalytic activities are observed to change from 1 to 3 orders of magnitude depending on the active phase which suggests that the activity is not only related to the number of CUS. More complex factors involving the nature of the active sites influencing the relative stability of reactants, intermediates and transition states must be considered. It can also be observed that surface site concentrations remain comprised between 1.4 and 5.8 sites/nm^2 which may also explain why volcano curves have been reported in the literature by expressing activities by surface area.

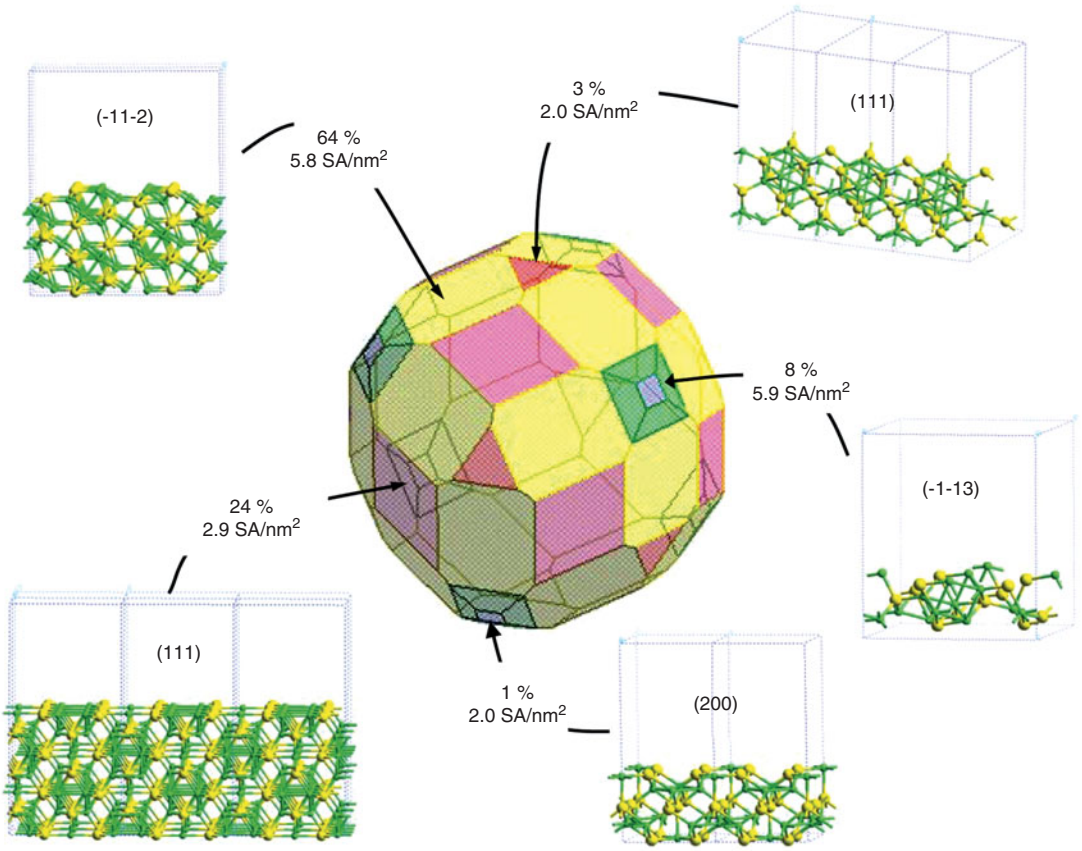

Figure 3

Morphological model of a Co_9S_8 particule. Color legend for the morphology pattern: pink: (011), green: (-1-13), blue: (200), yellow: (-11-2), red: (111). Color legend for the surface atomic cell: yellow balls: sulfur atoms, green balls: cobalt.

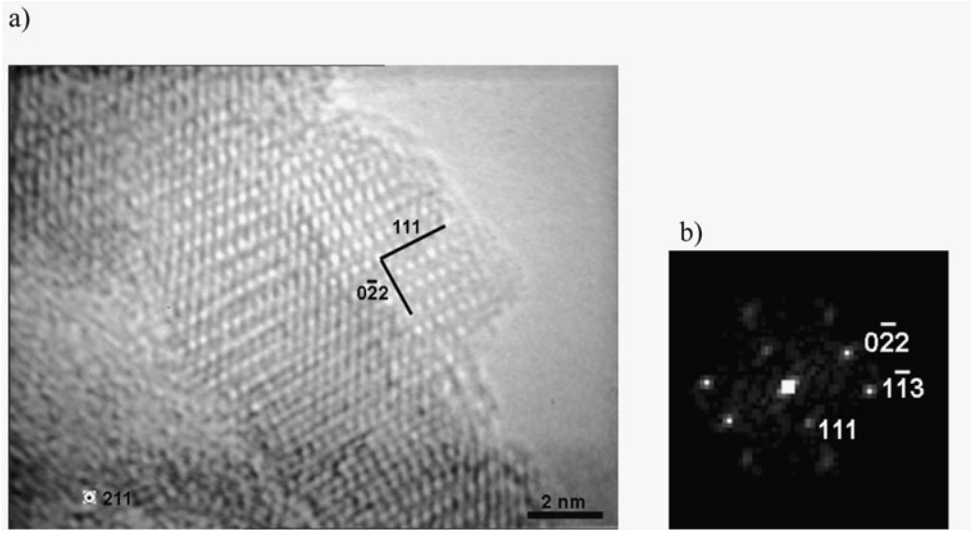

Figure 4

HRTEM image of Co_9S_8 alumina supported catalyst a) and his Fourier transform b).

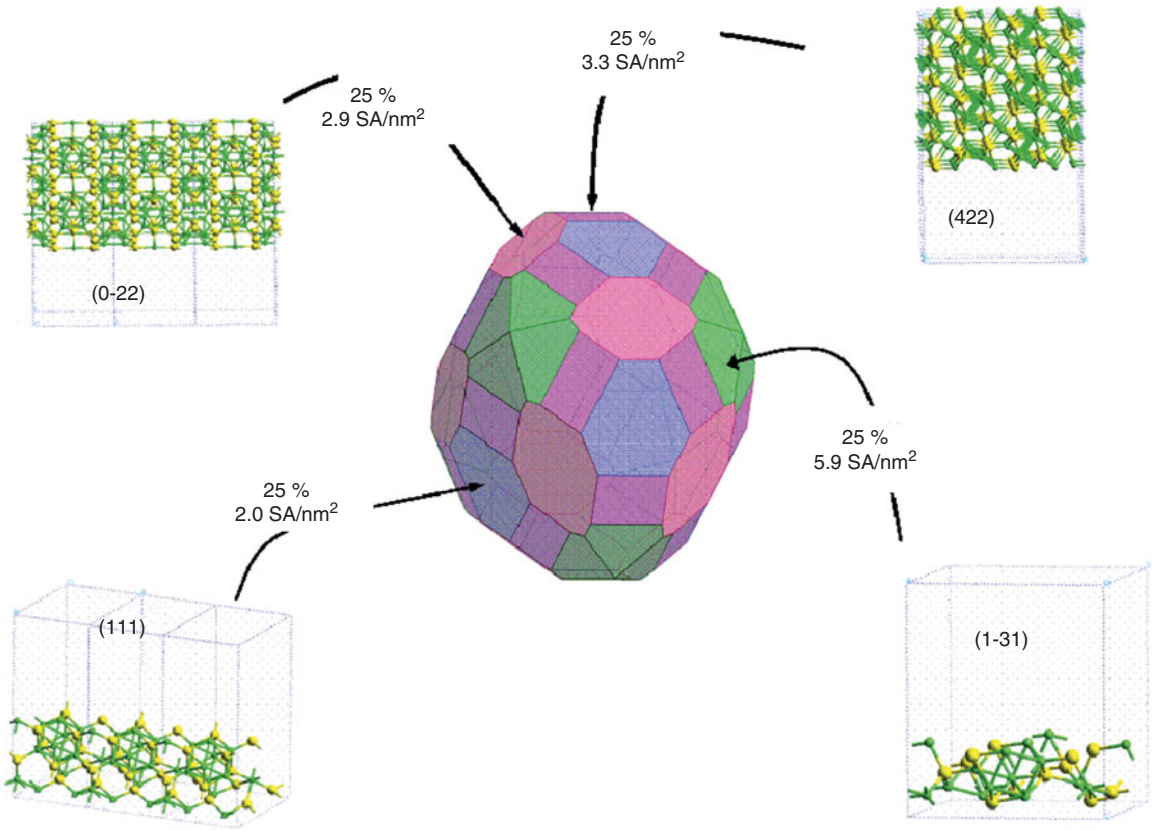

Figure 5

Morphological model of a Co_9S_8 alumina supported particle. Color legend for the morphology pattern: pink: (0-22), green: (1-31), blue: (111), magenta: (422).

2.3 Microkinetic Modeling

For hydrogenation and hydrodesulfurization reactions over sulfide catalysts, many kinetic studies have been carried out in the literature so far [11, 12, 25-29]. In the same spirit as [10, 25, 27], we have tested several relevant models and determined the model able to reproduce at best the experimental catalytic results obtained previously. In [15], we have applied a first model within the Langmuir-Hinshelwood formalism, which considers molecular adsorption for all species. H_2S is regarded as a pure inhibitor of the toluene hydrogenation reaction. A similar microkinetic model was already used in a previous work [9], putting forward a volcano curve relationships between HDS of DBT and *E(MS)*, the *ab initio* calculated sulfur-metal bond energies of the sulfide catalysts [7-9]. *E(MS)* appeared thus as a good chemical descriptor of the catalyst for recovering such a volcano. A second and more refined model (also called *model 6b* in [10]), is a one site model within the Langmuir-Hinshelwood formalism and assumes that H_2S and H_2 adsorb dissociatively at the surface. In this case, the sulfhydryl groups engendered by H_2S dissociation may also take part to the elementary steps of the reaction as earlier proposed by Kastzelan [10, 27]. In what follows we will focus on this microkinetic model to underline its improvement for the description of the toluene hydrogenation reaction. This model is optimized by expressing the adsorption constants and activation energies as a linear relationship of the sulfur-metal bond energies calculated by DFT in previous work [7-9]. It must be noticed that we have tested all other models reported in [10], however the one described in what follows appears as the best one.

2.3.1 Elementary Steps of the Mechanism

Equations (E1) to (E7) describe the relevant elementary steps of the mechanism involved in the one site (M^*) microkinetic model of toluene hydrogenation.

$$M^* + H_2S \xleftrightarrow{K_S} MS + H_2 \qquad \text{(E1)}$$

$$MS + M^* + H_2 \xleftrightarrow{K_{H_2}} MSH + MH \qquad \text{(E2)}$$

$$MS + M^* + H_2S \xleftrightarrow{K_{H_2S}} 2MSH \quad \text{(E3)}$$

$$M^* + R \xleftrightarrow{K_R} MR \quad \text{(E4)}$$

$$MR + MSH \xrightarrow{k_{SH}} MRH + MS \quad \text{(E5)}$$

$$MRH + MH \longrightarrow MRH_2 + M^* \quad \text{(E6)}$$

Step (E1) is the creation of MS species required for hydrogen and H_2S activation. This equation is also related to the sulfidation state of the catalytic surface depending on the sulfo-reductive conditions as revealed by DFT calculations [19, 20, 23, 24]. We cannot exclude that this state changes in various reaction conditions. Hydrogen and H_2S are both activated through heterolytic dissociation through steps (E2) and (E3). Step (E4) stands for the adsorption of toluene (labelled *R*) on the active sites. Step (E5) is the first hydrogen transfer from the sulfhydryl group to the adsorbed toluene and is assumed to be rate determining. Step (E6) is the second hydrogenation from MH group. In the models tested (not described here), this step was also supposed as being rate determining. However, this assumption does not provide a good fit of the experimental data. Subsequent elementary steps leading to methyl-cylclohexane occur as follows:

$$2M^* + H_2 \longrightarrow 2MH \quad \text{(E7)}$$

$$MRH_2 + MSH \longrightarrow MRH_3 + MS \quad \text{(E8)}$$

$$MRH_3 + MH \longrightarrow MRH_4 + M^* \quad \text{(E9)}$$

$$MRH_4 + MSH \longrightarrow MRH_5 + M \quad \text{(E10)}$$

$$MRH_5 + MH \longrightarrow MRH_6 + M^* \quad \text{(E11)}$$

$$MRH_6 \longrightarrow RH_6 + M^* \quad \text{(E12)}$$

These elementary steps ensure simultaneously the alcane formation and the partial regeneration of M* sites. In order to equilibrate the global reaction scheme (full M* recovery, avoiding H_2S over-consumption), the following final steps (occurring two times) are proposed:

$$2M^* + H_2 \longrightarrow 2MH \quad \text{(E13-E14)}$$

$$2MH + MS \longrightarrow 3M^* + H_2S \quad \text{(E15-E16)}$$

As a consequence, H_2S takes part to the reaction by producing the MS and MSH species at the surface and is regenerated at the end of the catalytic cycle so that it does not appear in the global reaction.

2.3.2 Equation Rates and Brønsted-Evans-Polanyi Relationships

Within the proposed mechanism, steps (E1) to (E4) are assumed to be equilibrated, whereas step (E5), corresponding to the addition of the first hydrogen from the sulfhydryl group, is rate determining. Many other assumptions (such as listed in [10]) have been checked: they all lead to less satisfactory results.

The equation of site conservation is written as follows:

$$\theta^* + \theta_S + \theta_{SH} + \theta_H + \theta_R = 1 \quad (5)$$

The reaction rate is finally expressed as:

$$\begin{aligned} r(T, p_{H_2S}, p_{H_2}) &= k_{SH}\theta_R\theta_{SH} \\ &= k_{SH}\frac{\alpha_R\alpha_S^{1/2}\alpha_{H_2S}^{1/2}}{(1+\alpha_S+\alpha_R+\alpha_S^{1/2}\alpha_{H_2S}^{1/2}+\alpha_{H_2}\alpha_S^{1/2}\alpha_{H_2S}^{-1/2})^2} \end{aligned} \quad (6)$$

$$\text{with } \alpha_S = \frac{p_{H_2S}}{K_S p_{H_2}} \quad \text{and} \quad \alpha_i = K_i\frac{p_i}{p^o} \quad (7)$$

In the same spirit as firstly proposed by Kasztelan [30], or more recently revisited by Toulhoat and Raybaud [9], we express the adsorption constant, K_i, and activation energy as a function of a relevant intrinsic parameter of the sulfide catalyst, the sulfur-metal bond energy, *E(MS)*, as defined in [7-9]. Similar approaches within the framework of ammonia synthesis on metal catalysts have been proposed recently [5, 31].

The adsorption constants, K_i, and the kinetic constant k_{SH} are thus written as:

$$K_i = e^{\Delta S_i/R - \Delta H_i/RT} = e^{\Delta S_i/R} e^{\left[\Delta E_{i,0} + \beta_i E(MS)\right]/RT} \quad (8)$$

$$k_{SH} = \frac{k_B T}{h} e^{-\Delta G^{\neq}/RT} = \frac{k_B T}{h} e^{-\left[\Delta G_0^{\neq} + \gamma_{SH} E(MS)\right]/RT} \quad (9)$$

where k_B and h are the Boltzmann and Planck's constants respectively.

If a linear relationship holds between the internal energy variation (resp. activation energy) and *E(MS)*, resulting from Brønsted-Evans-Polanyi (BEP) relationship [32-34], K_i and k_{SH} depend on the catalyst via *E(MS)* and the BEP parameters, β_i and γ_{SH}. We thus obtain an expression of r as a function of T, p_{H_2S}, p_{H_2}, *E(MS)*.

The BEP linear relationships used for the kinetic modelling are plotted in Figure 6. All adsorption energies are exothermic. The higher *E(MS)*, the stronger the interaction of the active free site M* with toluene, -S, -SH is.

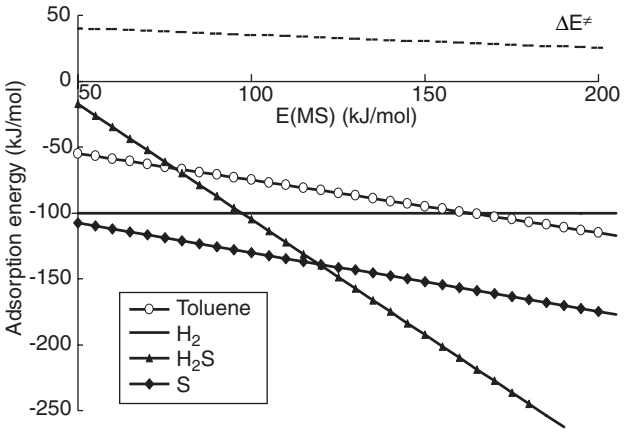

Figure 6

Linear BEP relationships between adsorption energies (and activation energies) and the sulfur-metal bond energies, *E(MS)*.

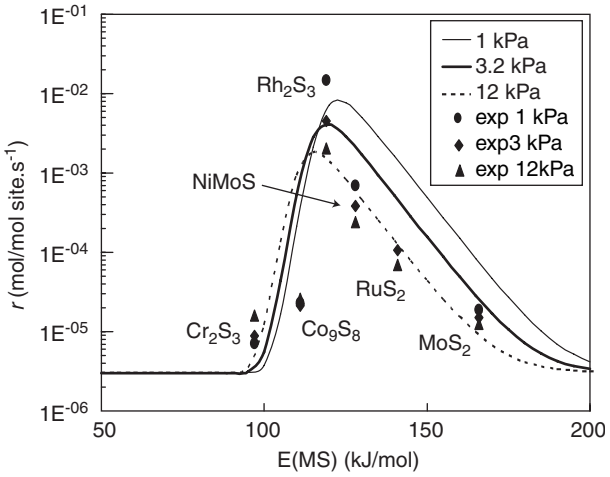

Figure 7

Experimental hydrogenation activity (particle size and shape corrected) plotted against sulfur-metal bond energies, *E(MS)*, for different partial pressure of H_2S: 1 kPa (circle), 3.2 kPa (diamond), 12 kPa (triangle). The kinetic model (6) fitting the experimental results are represented as a function of p_{H_2S}.

2.3.3 Volcano Curves and Surface Coverage

In Figure 7, it can be observed that the volcan curve as already proposed for DBT HDS in [7-9] is recovered for the toluene hydrogenation on the six tested sulfides catalysts. In our previous work [15], such a volcano was also obtained with a more simple model where the molecular adsorption of H_2 and H_2S was assumed. However, as found in [15], this model is not able to render the subtle promoting effect of H_2S on Cr_2S_3 and Co_9S_8 catalysts. We confirm that the optimal

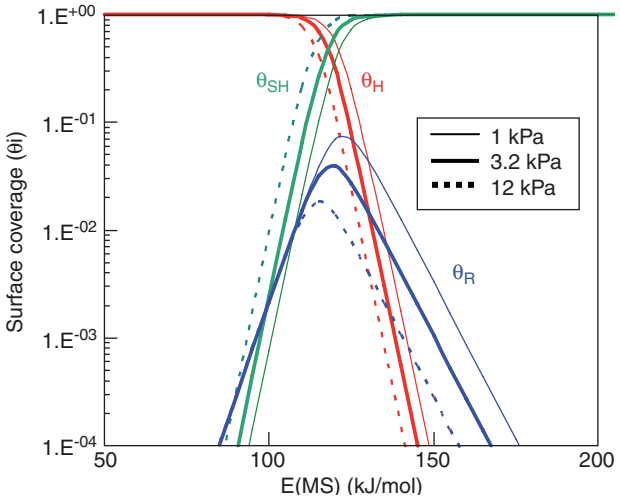

Figure 8

Surface coverage of the predominant species as a function of *E(MS)* and: toluene (θ_R), MSH (θ_{SH}) and MH (θ_H) species.

catalysts (Rh_2S_3 and NiMoS) are found for intermediate value of *E(MS)*. This result can be interpreted again within the framework of the Sabatier principle [1,8]. A careful analysis of the species coverages (*Fig. 8*) as a function of the *E(MS)* reveals that for high *E(MS)* the surface is saturated by MSH species. For low *E(MS)*, the surface is fully covered by MH species. In these two regions, the number of toluene molecules adsorbed on the surface is extremely low, and the rate law decreases abruptly (as expected from the rate equation (6) for very low θ_R value). For intermediate *E(MS)*, the toluene coverage reaches a maximum. Furthermore, the sulfhydryl species coverage is simultaneously high at the surface which maximizes the product $\theta_{SH}\theta_R$ and explains why the maximum of the hydrogenation rate law is reached close to the *E(MS)* value of Rh_2S_3. It can be noticed that, in this region, MH species occupy a non negligible fraction of catalytic sites. Hence, the optimal distribution of toluene, MSH and MH species for intermediate sulfur-metal bond strength explains why this region is optimal for catalysis as suggested earlier by Kasztelan [25].

2.3.4 Effect of p_{H_2S}

Figure 7 shows that for *E(MS)* values greater than 115 kJ/mol, the increase of the partial pressure of H_2S from 3.2 kPa to 12 kPa decreases the reaction rate. This inhibiting effect of H_2S, was observed experimentally on many sulfides such as MoS_2 [10]. However, as we pointed out in the previous section, for Cr and Co sulfides, H_2S has a promoting effect on the hydrogenation activity. After exploring many different possible mechanisms, we conclude that the positive effect of H_2S can only be recovered when the hydrogenation step involving H transfer from sulfhydryl groups (engendered

by H_2S dissociative adsorption) is rate determining. In particular, this effect cannot be observed with mechanisms where the rate determining step is the hydrogenation through MH species. The best model is also able to reproduce a volcano with a non symmetrical shape (more pronounced rate decrease at low *E(MS)*).

The effect of H_2S is also to shift the position of the optimal catalyst. More precisely, an increase of the partial pressure of H_2S implies a slight displacement of the volcano maximum towards weaker sulfur-metal bond energies. This displacement is explained by the impact of H_2S partial pressure on the surface coverages, as visualized in Figure 8. An increase of p_{H_2S} implies a shift of the maximum of the toluene surface coverage towards low *E(MS)*. At the same time, the crossing point of the MSH and MH species is also displaced towards lower *E(MS)*. The combination of both trends induces the shift of the volcano's maximum. This effect reveals that the optimal catalyst depends on the reaction conditions and tends to counteract the effect of p_{H_2S}. Furthermore, at low *E(MS)* increasing leads to higher SH surface coverages, whereas θ_R is moderately affected. This analysis explains why for higher p_{H_2S}, the HDS activity is enhanced on catalysts such as chromium and cobalt sulfides. Such an impact of the reaction conditions on the periodic trends of catalytic properties was proposed by Kasztelan in [25] who noticed that "the nature of the optimum solid will depend on the reactions conditions". Results obtained in the current work give a more quantitative and rational basis for understanding this trend.

CONCLUSIONS

HRTEM combined with molecular modeling was used to describe the sizes and morphologies of unsupported and supported Co_9S_8 as well as for Cr_2S_3, Rh_2S_3, RuS_2 and MoS_2 transition metal sulfides. γ-alumina support was found to interact strongly with the cobalt sulfide providing a preferential orientation. This HRTEM and molecular modeling approach provided an estimate of the number of potential active sites present on the various supported catalysts and furnished a more rigorous way for determining normalized turnover rates in hydrogenation of toluene. It was shown that the variation of the number of active sites is not able to account for the change in 3 orders of magnitude of turnover rates measured. This complete description of the morphology of the TMS is also the primary step required for further modeling of the reactivity and the understanding of the structure sensitivity of TMS surfaces.

The hydrogenation of toluene on unsupported and alumina supported catalysts was found to be slightly promoted by an increase of H_2S partial pressure for cobalt and chromium sulfides. The analysis of this peculiar effect of H_2S on the catalytic activity of the TMS series was performed by combining a LH approach and BEP relationships using the sulfur-metal bond energy *E(MS)* descriptor. From the various selected LH equations, the best volcano curve correlation was obtained by using a model based on the heterolytic dissociation of H_2 and H_2S, and the first toluene monohydrogenation from MSH group as the rate determining step of the reaction. The promoter effect of H_2S is explained by the increase of SH concentration for catalysts with low *E(MS)* values such as Co_9S_8 and Cr_2S_3. This positive effect of H_2S can only be recovered when the hydrogenation step involving H transfer from sulfhydryl groups (engendered by H_2S dissociative adsorption) is rate determining. In contrast, this effect cannot be observed with mechanisms where the rate determining step is the hydrogenation through MH species. The second effect of p_{H_2S} is to displace the position of the volcano curve's maximum. This maximum moves in direction of catalysts with *E(MS)* values counteracting the effect of p_{H_2S}. This result puts forward that the optimal catalyst for toluene hydrogenation depends on the reaction conditions.

ACKNOWLEDGEMENTS

The authors would like to be grateful to Hervé Toulhoat at IFP for fruitful discussions. We also acknowledge one of the reviewer for very constructive remarks. N. Guernalec thanks IFP and CNRS for financial support.

REFERENCES

1 Sabatier, P. (1911) Hydrogénations et Déshydrogénations par Catalyse. *Berichte Deut. Chem. Gesellschaft* **44**, 2001.

2 Balandin, A.A. (1958) The Nature of Active Centers and the Kinetics of Catalytic Dehydrogenation. *Adv. Catal.* **10**, 96-129.

3 Boudart, M. (1997) *Handbook of Heterogeneous Catalysis*, Wiley-VCH, Weinheim.

4 Ichikawa, S. (1988) Heterogeneous Catalysis with Non-uniformly Reactive Adsorbates. *J. Phys. Chem.* **92**, 6970.

5 Logadottir, A., Rod, T.H., Nørskov, J.K., Hammer, B., Dahl, S., Jacobsen, C.J.H. (2001) The Brønsted-Evans-Polanyi Relation and the Volcano Plot for Ammonia Synthesis over Transition Metal Catalysts. *J. Catal.* **197**, 229-231.

6 Chianelli, R.R., Berhault, G., Raybaud, P., Kasztelan, S., Hafner, J., Toulhoat, H. (2002) Periodic trends in hydrodesulfurization: in support of the Sabatier principle. *Appl. Catal. A-Gen.* **227**, 83.

7 Raybaud, P., Hafner, J., Kresse, G., Toulhoat, H. (1997) *Ab initio* Density Functional Studies of Transition-Metal Sulphides: I. Crytal Structure and Cohesive Properties. *J. Phys. Condens. Mat.* **9**, 11085-11106.

8 Toulhoat, H., Raybaud, P., Kasztelan, S., Kresse, G., Hafner, J. (1999) Transition Metals to Sulfur Binding Energies Relationship to Catalytic Activities in HDS: Back to Sabatier with First Principle Calculations. *Catal. Today* **50**, 629-636.

9 Toulhoat, H., Raybaud, P. (2003) Kinetic Interpretation of Catalytic Activity Patterns Based on Theoretical Descriptors. *J. Catal.* **216**, 63-72

10 Kasztelan, S., Guillaume, D. (1994) Inhibiting Effect of H_2S on Toluene Hydrogenation over a MoS_2/Al_2O_3 Catalyst. *Ind. Eng. Chem. Res.* **33**, 203. Erratum (1995) *Ind. Eng. Chem. Res.* **34**, 1500.

11 Olguin Orozco, E., Vrinat, M. (1998) Kinetics of Dibenzothiophene Hydrodesulfurization over MoS_2 Supported Catalysts: Modelisation of the H_2S partial Pressure Effect. *Appl. Catal. A-Gen.* **170**, 195-206.

12 Blanchin, S., Galtier, P., Kasztelan, S., Kressmann S., Penet, H., Perot, G. (2001) Kinetic Modeling of the Effect of H_2S and of NH_3 on Toluene Hydrogenation in the Presence of a $NiMo/Al_2O_3$ Hydrotreating Catalyst. Discrimination between Homolytic and Heterolytic Models. *J. Phys. Chem.* **105**, 10860-10866.

13 Hensen, E.J.M., Brans, H.J.A., Lardinois, G.M.H.J., De Beer, V.H.J., Van Veen, J.A.R., Van Santen, R.A. (2000) Periodic Trends in Hydrotreating Catalysis: Thiophene Hydrodesulfurization over Carbon-Supported 4d Transition Metal Sulfides. *J. Catal.* **192**, 98-107.

14 Hermann, N., Brorson, M., Topsøe H. (2000) Activities of Unsupported Second Transition Series Metal Sulfides for Hydrodesulfurization of Sterically Hindered 4,6-Dimethyldibenzothiophene and of Unsubstituted Dibenzothiophene. *Catal. Lett.* **65**, 169-174.

15 Guernalec, N., Cseri, T., Raybaud, P., Geantet, C., Vrinat, M. (2004) Influence of H_2S on the Hydrogenation Catalytic Activity of Relevant Transition Metal Sulfides. *Catal. Today* **98**, 61-66.

16 Bezverkhyy, I, Danot, M., Afanasiev, P. (2003) New Low-Temperature Preparations of Some Simple and Mixed Co and Ni Dispersed Sulfides and Their Chemical Behavior in Reducing Atmosphere. *Inorg. Chem.* **42**, 1764-1768.

17 De Los Reyes, A., Vrinat, M., Geantet, C., Breysse, M. (1991) Ruthenium Sulphide Supported on Alumina Catalysts: Physicochemical Characterization and Catalytic Properties in Hydrogenation Reactions. *Catal. Today* **10,** 645.

18 Surface Builder Crystal builder, Morphology modules distributed within the Cerius^2 (release 4.8.1) and Materials Studio (release 4.0) package by Accelrys (http://www.accelrys.com).

19 Raybaud, P., Hafner, J., Kresse, G., Kasztelan, S., Toulhoat, H. (2000) *Ab Initio* Study of the H_2-H_2S/MoS_2 Gas-Solid Interface: The Nature of the Catalytically Active Sites. *J. Catal.* **189**, 129-146.

20 Raybaud, P., Hafner, J., Kresse, G., Kasztelan, S., Toulhoat, H. (2000) Structure, Energetics, and Electronic Properties of the Surface of a Promoted MoS_2 Catalyst: An ab Initio Local Density Functional Study. *J. Catal.* **190**, 128-143.

21 Grillo, M.E., Smelyanski, V., Sautet, P., Hafner, J. (1999) Density Functional Study of the Structural and Electronic Properties of $RuS_2(111)$. I. Bare Surfaces. *Surf. Sci.* **439**, 163-172.

22 Grillo, M.E., Sautet, P. (2000) Density Functional Study of the Structural and Electronic Properties of $RuS_2(111)$. II. Hydrogenated Surfaces. *Surf. Sci.* **457**, 285-293.

23 Schweiger, H., Raybaud, P., Kresse, G., Toulhoat, H. (2002) Shape and Edge Sites Modifications of MoS_2 Catalytic Nanoparticles Induced by Working Conditions: A Theoretical Study. *J. Catal.* **207**, 76-87.

24 Schweiger, H., Raybaud, P., Toulhoat, H. (2002) Promoter Sensitive Shapes of Co(Ni)MoS Nanocatalysts in Sulfo-Reductive Conditions. *J. Catal.* **212**, 33-38.

25 Kasztelan, S. (1989) The Importance of Active Site Structure on the Appearance of Periodic Trends of Catalytic Properties. *Catal. Lett.* **2**, 165.

26 McGarvey, G.B., Kasztelan, S. (1994) An Investigation of the Reduction Behavior of MoS_2/Al_2O_3 and the Subsequent Detection of Hydrogen on the Surface**.** *J. Catal.* **148**, 149-156.

27 Kasztelan, S. (1996) *Hydrotreating Technology for Pollution Control*, Marcel Dekker Inc., New-York.

28 Girgis, M.J., Gates, B.C., Michael, J., Bruce, C. (1991) Reactivities, Reaction Networks, and Kinetics in High-Pressure Catalytic Hydroprocessing. *Ind. Eng. Chem. Res.* **30**, 2021-2058.

29 Vrinat, M.L. (1983) The Kinetics of the Hydrodesulfurization Process - a Review. *Appl. Catal.* **6**, 137-158.

30 Kasztelan, S. (1992) Kinetic Interpretation of Periodic Trends in Heterogeneous Catalysis. *Appl. Catal. A-Gen.* **83**, L1-L5.

31 Bligaard, T., Nørskov, J.K., Dahl, S., Matthiesen, J., Christensen, C.H., Sehested, J., (2004) The Brønsted-Evans-Polanyi Relation and the Volcano Curve in Heterogeneous Catalysis. *J. Catal.* **224**, 206-217.

32 Brønsted, J.N., Pedersen, K.J. (1924) The Catalytic Decomposition of Nitramide and its Physico-Chemical Applications. *Z. Phys. Chem.* **108**, 185-235.

33 Evans, M.G., Polanyi, M. (1936) Further Considerations of the Thermodynamics of Chemical Equilibria and Reaction Rates. *T. Faraday Soc.* **32**, 1333-1360.

34 Evans, M.G., Polanyi, M. (1938) Inertia and Driving Force of Chemical Reactions. *T. Faraday Soc.* **34,** 11-24.

Manuscript final received in July 2006